Numerical and experimental study of a multimode optical fiber sensor based on Fresnel reflection at the fiber tip for refractive index measurement

Antoine Brientin, Dominique Leduc, Virginie Gaillard, Marion Girard, Cyril Lupi

Numerical and experimental study of a multimode optical fiber sensor based on Fresnel reflection at the fiber tip for refractive index measurement

Antoine Brientin[*,a], Dominique Leduc[a], Virginie Gaillard[a,c], Marion Girard[b], Cyril Lupi[a]

[a] *Institut de recherche en Génie Civil et Mécanique, GeM-TRUST, UMR CNRS 6183, University of Nantes, France, 2 Chemin de la Houssinière, 44300 Nantes, France*

[b] *Institut de recherche en Génie Civil et Mécanique, GeM-E3M, UMR CNRS 6183, University of Nantes, France, 58 Rue Michel Ange, 44600 Saint Nazaire, France*

[c] *Icam - Site de Nantes, 35 Avenue du Champ de Manoeuvres, 44470 Carquefou*

Abstract

This paper presents the numerical and experimental study of a multimode optical fiber (MMF) sensor based on Fresnel reflection at the fiber tip. Considering different modal power distributions (uniform mode distribution, gaussian and equilibrium mode distribution), the effective fraction of the incident light reflected at the interface between the end of the fiber and the surrounding medium is first calculated numerically with a ray model. Even when considering modal power distribution and non-normal incidence influence, simplifying assumptions such as normal incidence hypothesis can be made to facilitate experimental data exploitation, with a maximum error on the deduced medium refractive index of the 10^{-4} order. A statistical analysis of noise is then made, to study the influence of a random noise between 0.1% and 5% noise level: results show that the approximation error made by using normal incidence formula for a Fresnel sensor based on a MMF is significantly smaller than the repeatability error. These assumptions are then verified experimentally with two experimental setups by measuring the refractive index at 1550 nm of reference solutions (distilled water-isopropanol and distilled water-sodium chloride mixtures) with a Fresnel based on a multimode fiber, and a Fresnel based on single-mode fiber for comparison. Good agreement is found with refractive index values from the literature with a maximum relative difference of only 0.1%, and the maximum experimental uncertainties in this work is 1.1×10^{-4}. Differences between refractive index measured with a Fresnel based on single-mode and multimode fiber are found to be in accordance with values from the statistical study.

Key words: Fresnel sensor, Multimode fiber, Chemical species sensor

1. Introduction

The Fresnel sensor based on a cleaved single-mode fiber has proven to be an accurate intrinsic refractive index measurement system, as detailed in the following. This sensor relies on the Fresnel reflection at the interface between the end of a single-mode fiber (SMF) and a unknown medium to determine the refractive index of the latter thanks to Fresnel formulas [1]. The reason for the predominant use of SMF in Fresnel sensors is related to light properties inside the optical fiber. Inside a fiber, electromagnetic field distribution is often studied under the mode concept, which represents the various patterns of propagation inside the waveguide. From a physical standpoint, waveguide modes are transverse field patterns with a periodic dependence along the longitudinal axis of the fiber, created by the constructive interferences of the repeatedly reflected electromagnetic waves with themselves. From a purely mathematical point a view, they are the equations of the planes waves that can propagate inside the fiber, such expressions being obtained by first solving the propagation equation to obtain general formulations of the transverse electromagnetic fields and then solving the boundary conditions in the fiber, at the core/cladding interface, to obtain the exact expressions associated with each mode. Because of the opto-geometric characteristics of the fiber, the SMF has the particularity to propagate

*Corresponding author

Email address: antoine.brientin@univ-nantes.fr (Antoine Brientin)

only the fundamental mode, hence its name. This mode has the particularity to propagate parallel to fiber axis [2], which can have some useful consequences on the Fresnel coefficients that describe the fraction of light that will be reflected by the surrounding medium at the end of the fiber: if the fiber is cut perpendicular to the propagation axis, Fresnel coefficients can be reduced to their simple expression at normal incidence. As they are functions of the refractive indexes on both side on the interface, if the fiber refractive index is known, this allows for an easy retrieval of the unknown medium refractive index. Because this optical property characterizes the response at the atomic level of the medium to light excitation [3], measuring the refractive index is a way to retrieve information on a medium such as the atomic elements composing it, its temperature or pressure. Various measurements can therefore be made simply by immersing the fiber tip into a medium and then measuring the power reflected in the fiber to deduce a refractive index, giving the Fresnel sensor a wide range of applications. This even works in a mixture, where the effective refractive index can be related to the fraction of components, with rules such as Clausius-Mossotti, Maxwell-Garnett or Bruggeman formulas [4].

For example, [5] demonstrated that a Fresnel sensor is capable of distinguishing carbon dioxide or methane bubbles in flowing pressurized seawater, allowing for example long distance surveys in underwater drilling wells. [6] proved volatile organic compounds detection capabilities, with a Fresnel sensor where the cleaved fiber tip was covered with a zeolite thin film, whose micro-porous structure allows for gas molecules adsorption, changing its effective refractive index. Using a similar principle, [7] used a fiber tip coated with a sensing membrane to measure cadmium ions (Cd^{2+}) in water, using the interactions of the ions with the coating. Some other applications include localized measurement of curing reaction [8, 9, 10], water diffusion monitoring [11], phase change detection [12], pH measurement [13] or temperature measurement because of the thermo-optic properties of the medium [14]. Fresnel sensor is often use to measure concentration of chemical species in biochemical industries, but also to monitor engineering processes: determination of alcohol, glucose or sodium chloride content in a water solution is well-documented, and these mixtures are often used to demonstrate the sensing capabilities of a refractive index measurement system, including the Fresnel sensor. [15] used such a sensor to measure the concentration of an NaCl-H_2O liquid, using an arrayed waveguide grating for multipoint measurements. As each sensing head was constituted of two fibers, with one of them being covered in a thermo-optic material, simultaneous concentration and temperature measurement of the sample was possible. [16] used a Fresnel sensor to study ethanol samples from 0% to 100% water content, at 1310 nm and 1550 nm. Such measurements, where the non-linear evolution of the refractive index of a water-ethanol mixture is easily seen, have direct applications, like real-time monitoring of bioethanol fabrication process. To obtain measurement at long distances, [17] used an Optical Time-Domain Reflectometer as an combined light source and detector, to measure the refractive index of glycerol/distilled water and alcohol/distilled water solutions, the OTDR giving additional information about the signal attenuation along the fiber.

Measurement with a Fresnel sensor probes a $2\pi r\lambda$ volume at the fiber tip, with λ the wavelength (1530 to 1560 nm range for the dominant spectral region used in long-distance telecommunications) and r the radius of the fiber core (4 μm for a standard single-mode fiber). When measurements are made in medium with an arbitrary property gradient, this small probing size may be an advantage [18], as it allows to measure refractive index at specific locations. However, it is then very localized, which make it extremely sensible to perturbations, e.g. air bubble inside a resin when monitoring curing or impurities in solution when measuring chemical species. This is a major drawback if one want to measure the effective refractive index of a mixture or a heterogeneous medium. In order to have more confidence on the measured refractive index, it is necessary to heavily increase the probing volume, and consequently to use other type of fiber than the single-mode fiber, whose small core radius is a limiting factor. Also, if one want to make measures inside a structure subject to significant elongation, such as synthetic mooring cables, brittle behaviour low elongation at break of silica fibers are also problematic.

Using multimode fiber (MMF) as a sensor based on Fresnel reflection at fiber tip could significantly enlarge the probed volume because of their core diameter, much larger than SMF ones. Plastic optical fibers are highly multimode because of their large core diameter, but have low costs and lower elastic modulus than glass optical fibers, which make them attractive for some industrial applications. They also have a larger elongation at break, which may make them useful for monitoring of cables subject to large strain [19]. Even though most of Fresnel sensors use standard SMF, a few applications use MMF to measure a refractive index, but rather rely on an etched fiber and the loss of total internal reaction [20, 21] rather than on the reflection at the fiber tip; the same principle has also been applied to plastic optical fibers by [22]. A question then arises, whether a multimode fiber is suitable as a Fresnel sensor based on reflection at the fiber tip, as the large number of modes propagating inside the fiber implies several refractive indexes for the

fiber, as well as changes in the incidence angles on the interface. If multimode fibers were proven to be usable, this would allow to overcome one of the main drawbacks of the Fresnel sensor on a SMF, its small probing volume. In this paper, a new ray model is formulated, that takes into account changes of the Fresnel coefficients with non-normal incidence on the interface, modal power distribution, dispersion and spectral power distribution. The advantages of this model are threefold: it is easily usable on fibers with different characteristics, combines the numerous effects that are to be taken into account for a multimode fiber, and at the same time allows for accurate calculation of a medium's refractive index. To the best of author's knowledge, combining these effects into a formula which also allows for easy experimental data exploitation has never been done before. The aim of this paper is firstly to determine numerically if normal incidence hypothesis and related formulas can still be used without significant precision loss, which would facilitate experimental data exploitation and refractive index determination. A statistical analysis of noise is also performed in order to evaluate measurement uncertainties. Experimental confirmation of the MMF Fresnel sensor capabilities is based on isopropanol and sodium chloride content measurement in a distilled water solution.

2. Fresnel sensor and multimode fiber implications

2.1. Working principle of the Fresnel sensor in a single-mode fiber

A Fresnel sensor is a simple refractive index measurement system created by cleaving an optical fiber perpendicular to the propagation axis. At this interface between the fiber tip and the surrounding medium, a fraction of the incident power (P_i) is transmitted in the medium (noted P_t), whereas a small part is reflected (P_r), as illustrated in figure 1.

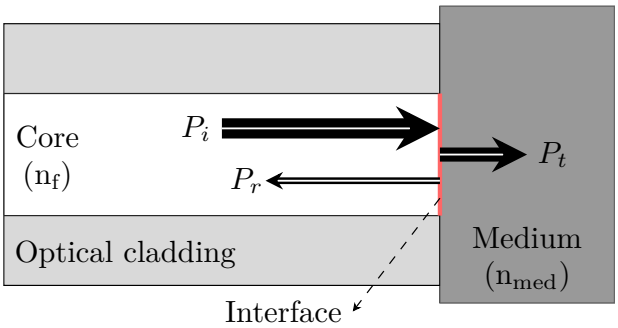

Figure 1: Working principle of an optical fiber sensor based on Fresnel reflection at the fiber tip

The fraction of reflected light is related to the fiber and medium refractive indexes (n_f and n_{med}, respectively) by the Fresnel coefficients [1]. As Fresnel sensors are commonly made with standard single-mode fibers, where the only propagating mode travels parallel to the fiber axis [2], Fresnel coefficients are therefore simplified to their expression at normal incidence, leading to [1]:

$$\frac{P_r}{P_i} = \left(\frac{n_f - n_{\text{med}}}{n_f + n_{\text{med}}}\right)^2 \tag{1}$$

A simple setup for measurements with a Fresnel sensor is presented in figure 2. Light from the laser passes through the coupler, being divided between a reference fiber and a measurement fiber. At the end of the measurement fiber (1) is the cleaved fiber tip. At the end of the reference fiber (2), a detector can be used to monitor the stability of the light source and correct power fluctuations. The signal reflected at the fiber/medium interface is guided back to the coupler, being splitted a second time and finally recorded by the detector.

The measurement is based on the ratio between the power reflected by a known medium such as air and the power reflected by the unknown medium [23]. Measurements lead to two similar equations, with K_{att} an attenuation coefficient representing all losses in the system, n_a the air index, here at a known and constant temperature. Combining

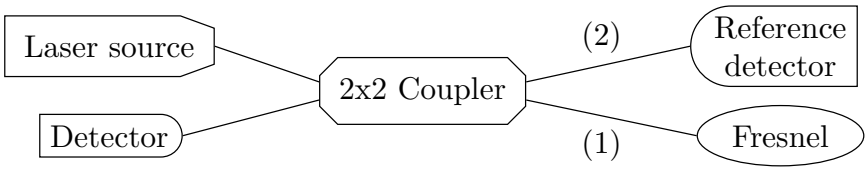

Figure 2: Minimal experimental setup for a Fresnel sensor

them, one can obtain, assuming that P_i and K_{att} are the same for the two measurements:

$$\frac{P_{\text{r,med}}}{P_{\text{r,air}}} = \frac{K_{\text{att}}\left(\frac{n_f - n_{med}}{n_f + n_{med}}\right)^2}{K_{\text{att}}\left(\frac{n_f - n_{\text{a}}}{n_f + n_{\text{a}}}\right)^2} \tag{2}$$

This leads to:

$$n_{\text{med}} = \begin{cases} n_f \dfrac{1-\eta}{1+\eta} & \text{if } n_{\text{med}} < n_f \\ n_f \dfrac{1+\eta}{1-\eta} & \text{if } n_{\text{med}} > n_f \end{cases} \tag{3}$$

with:

$$\eta = \frac{n_f - n_a}{n_f + n_a}\sqrt{\frac{P_{\text{r,med}}}{P_{\text{r,air}}}} \tag{4}$$

2.2. Fresnel sensor on a multimode fiber

Using a multimode fiber as a Fresnel sensor involves changes in the mathematical retrieving of the medium refractive index, as modal power distribution needs to be considered. All the optical modes propagating in the optical fiber do not necessarily carry the same power, as a direct consequence of the wave equation's solutions and mode coupling [2]. To help determine the effects of modal power distribution (i. e. the optical power carried by each propagating mode) on the reflected power, each mode will be related to a ray with a propagation angle α, measured from the fiber axis: it has been shown that this ray model is satisfactory to represent the continuum of plane waves [24]. Power distributions will be written as $P_i(\alpha)$, a function of the propagation angle and therefore the incidence angle on the fiber/medium interface at the end of the fiber. The three main power distributions that can be found in the literature are:

- Uniform mode distribution (UMD): the power is uniformly distributed between all the modes, which means that $P_i(\alpha)$ is a constant. Because of mode coupling, which is the exchange of energy between modes, this distribution is very quickly lost [25]. Consequently, this distribution does not really reflect reality but is often considered as a first approach because of its simplicity. Moreover, it will also be a limit case for the following study, as large incidence angles will have the same weight as small ones in the calculations.

- Gaussian distribution: this widely used distribution represents a gaussian laser beam as a source. If the laser is aligned with the propagation axis of the fiber, the incident power can be expressed by:

$$P_i(\alpha) = \mathrm{e}^{-\frac{1}{2}\left(\frac{\alpha}{\sigma}\right)^2} \tag{5}$$

  With σ the standard deviation of the laser energy distribution, related to the full width at half maximum (FWHM) by FWHM $= 2\sqrt{2\ln 2}\sigma \approx 2,355\sigma$.

- Equilibrium mode distribution: this distribution takes into account the mode coupling phenomenon. This coupling is usually caused by fiber bending or microscopic imperfections of the optical core which cause the wave to scatter, resulting in a part of its energy being transferred to another mode. The equation giving the evolution of the power at a certain angle, considering modal attenuation and mode coupling is [24]:

$$\frac{\partial P(\alpha, z)}{\partial z} = -A(\alpha)P(\alpha, z) + \frac{\delta\alpha^2}{\alpha}\frac{\partial}{\partial\alpha}\left[\alpha C(\alpha)\frac{\partial P(\alpha, z)}{\partial\alpha}\right] \tag{6}$$

with $P(\alpha, z)$ the power inside the fiber at a distance z from the source and at the incidence angle α. $C(\alpha)$ is the coupling coefficient and $A(\alpha)$ the modal attenuation. The profile of the power distribution is therefore highly dependent on the coupling coefficient, the initial distribution, and the length of fiber. After a certain length (a few hundred meters for silica fibers, a few tens of meters for polymer fibers [26]), a stable state is reached, from which the energy distribution does not change anymore. Neglecting the attenuation losses in the fiber due to the short lengths involved, the power in unpolarized light based on a gaussian input, as a function of the angle of incidence is expressed by [27]:

$$P_i(\alpha) = J_0\left(2,405\frac{\alpha}{\alpha_{\max}}\right) \tag{7}$$

with J_0 the Bessel function of the first kind and integer order zero and $\alpha_{\max}$ the maximum incidence angle.

Figure 3 illustrates the difference between the three modal power distributions, for an maximum incidence angle of 8°; the total power of each distribution, i.e. the integrals up to $\alpha_{\max}$, is unitary and $\sigma = 1.48°$ for the gaussian distribution.

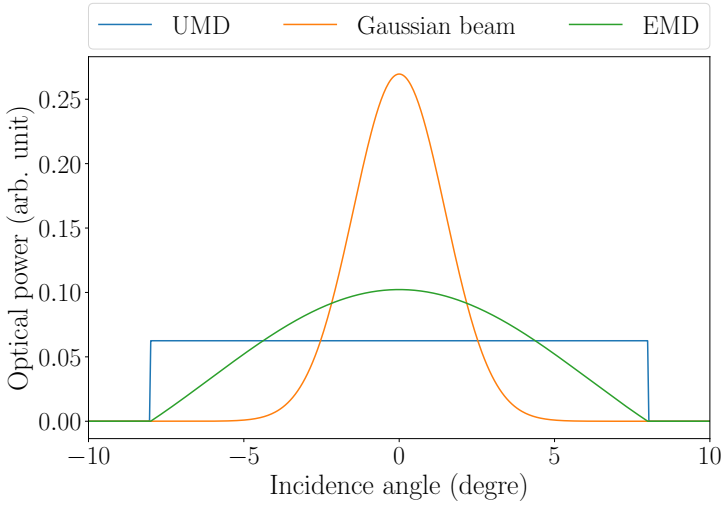

Figure 3: Illustration of the three described modal power distributions, with an 8° maximum incidence angle

As the normal incidence hypothesis can not be made anymore, because of the large optical core diameter and the ray model with numerous propagating modes, the Fresnel coefficients giving the fraction of the power reflected at the interface now depends on the incidence angle α and the polarization of the incident light [1]:

$$R_\perp = \left(\frac{n_f \cos\alpha - n_{\text{med}} \cos\alpha_{\text{med}}}{n_f \cos\alpha + n_{\text{med}} \cos\alpha_{\text{med}}}\right)^2 \tag{8}$$

$$R_\parallel = \left(\frac{n_f \cos\alpha_{\text{med}} - n_{\text{med}} \cos\alpha}{n_f \cos\alpha_{\text{med}} + n_{\text{med}} \cos\alpha}\right)^2 \tag{9}$$

where $R_\perp$ and $R_\parallel$ are the coefficients for perpendicular and parallel polarization, respectively. The refracted ray angle α_{med} is related to the incidence angle α by Snell-Descartes law. Because of the ray model, a single refractive index

is used for the fiber. At the α incidence angle, considering an arbitrary incident power on the interface $P_i(\alpha)$, the reflected power $P_r(\alpha)$ is then given by:

$$P_r(\alpha) = P_{i,\perp}(\alpha)R_\perp(\alpha) + P_{i,\parallel}(\alpha)R_\parallel(\alpha) \tag{10}$$

where $P_{i,\perp}(\alpha)$ and $P_{i,\parallel}(\alpha)$ are the incident powers for $\perp$ polarization and $\parallel$ polarization, respectively. For unpolarized light, the total power is evenly distributed between the two polarisation states [3], and the previous equation becomes:

$$P_r(\alpha) = \frac{P_i(\alpha)}{2}R_\perp(\alpha) + \frac{P_i(\alpha)}{2}R_\parallel(\alpha) \tag{11}$$

The total power reflected at the interface will therefore be given by integrating on all angles up to α_{max}, the maximum incidence angle on the interface, which depends on the opto-geometric characteristics of the optical fiber. Introducing K_{att} as a global attenuation coefficient representing all optical losses in the system, the measured reflected power is, based on equation from [24]:

$$P_r = 2\pi K_{\text{att}} \int_0^{\alpha_{max}} \frac{1}{2} Pi(\alpha) \left(R_\perp(\alpha) + R_\parallel(\alpha)\right) \sin(\alpha) d\alpha \tag{12}$$

The previous equations also suppose a monochromatic source, as a single refractive index of the optical fiber is used. For a multi-wavelength source, the refractive index of the medium depends on the wavelength used, thus having a influence on the Fresnel coefficients. Depending on the light source used, power may not be uniformly distributed over all wavelengths, and the incident power is therefore dependent of the incidence angle and the wavelength. For a source emitting between two wavelengths λ_1 and λ_2, equation (12) can be modified to also integrate between these values, leading to:

$$P_r = 2\pi K_{\text{att}} \int_{\lambda_1}^{\lambda_2} \int_0^{\alpha_{\max}} \frac{1}{2} Pi(\alpha, \lambda) \left(R_\perp(\alpha, \lambda) + R_\parallel(\alpha, \lambda)\right) \sin(\alpha) d\alpha d\lambda \tag{13}$$

This leads to a new expression of the ratio of the power reflected in the air and in the unknown medium:

$$\frac{P_{\text{r,med}}}{P_{\text{r,air}}} = \frac{\displaystyle\int_{\lambda_1}^{\lambda_2} \int_0^{\alpha_{max}} \frac{1}{2} P_i(\alpha, \lambda) \left(R_{\perp,med}(\alpha, \lambda) + R_{\parallel,med}(\alpha, \lambda)\right) \sin(\alpha) d\alpha}{\displaystyle\int_{\lambda_1}^{\lambda_2} \int_0^{\alpha_{max}} \frac{1}{2} P_i(\alpha, \lambda) \left(R_{\perp,air}(\alpha, \lambda) + R_{\parallel,air}(\alpha, \lambda)\right) \sin(\alpha) d\alpha} \tag{14}$$

where $R_{\perp,\text{air}}$ and $R_{\perp,\text{med}}$ are the Fresnel power coefficients for perpendicular polarization, at a fiber/air interface and fiber/medium interface, respectively; the same applies for parallel polarization. This equation, where the unknown is the refractive index of the medium n_{med}, is much more complex to solve, as $P_i(\alpha, \lambda)$ can take various forms, and there is no analytical expression directly giving n_{med}, unlike the simple case of normal incidence. Nevertheless, numerical tools make it easy to solve this equation in order to determine the desired index.

3. Numerical calculation of the effective reflected power

3.1. Method used and results

To determine the effective fraction of light reflected by the fiber/medium interface at the end of a multimode fiber, a Python program is used to calculate the reflected power according to equation (13) with zero losses and a unitary incident power on the solid angle. The refractive index of the core used was chosen to be 1.4682 at 1550 nm, a standard value for commercially available step-index silica optical fiber and dispersion was taking into with a mixed Sellmeier law for GeO_2-SiO_2 glasses, with coefficients from [28]. To implement a realistic distribution of the power over all wavelengths, the optical spectrum of a GN Nettest Fiberwhite (an amplified spontaneous emission source) was obtained experimentally with an Anritsu MS9710B optical spectrum analyser. Power was discretized over 100 wavelengths between 1520 nm and 1570 nm, and normalized to have a unitary power over the whole spectrum as represented in figure 4. Calculations were made for three numerical apertures (NA) from commercially available multimode fiber, which has a direct influence on the maximum incidence angle $\alpha_{\max}$ (see table 1).

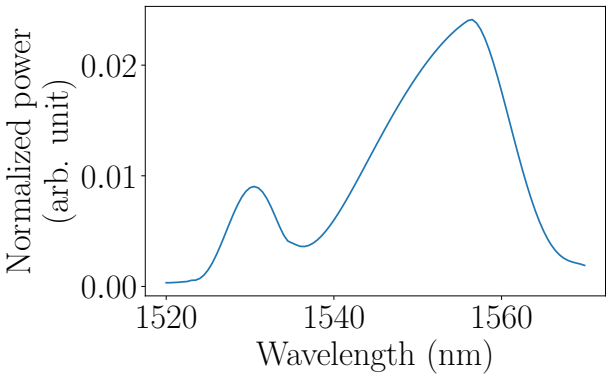

Figure 4: Discrete and normalized optical spectrum of a GN Nettest Fiberwhite ASE source

NA	θ_{max}	α_{max}
0.22	12.7°	8.7°
0.39	22.9°	15.5°
0.5	30.0°	20.1°

Table 1: Characteristics of the optical fibers, θ_{max} is the acceptance angle of the fiber and α_{max} the maximum incidence angle at the fiber/medium interface

All three previously described modal power distributions (uniform, gaussian and Bessel distributions) were studied, as well as four refractive indexes for the surrounding medium with temperature being considered constant at 25°C, to verify the consistency of the results over a large range:

- 1.0003 as the refractive index of air;
- 1.3180 as the refractive index of water at 1550 nm [29];
- 1.5 to approximately represent an aqueous solution with high concentration of sucrose or glucose [30], as well as mineral oils [31];
- 1.7 as an arbitrary example of a liquid with a high refractive index [32].

The relative difference, in %, between the Fresnel power coefficient at normal incidence (R_{SMF}, used for Fresnel on a single-mode fiber) and the numerically calculated effective fraction of light reflected at the interface (R_{MMF}) is defined as:

$$\frac{R_{MMF} - R_{SMF}}{R_{MMF}} \times 100 \tag{15}$$

These values are displayed in figure 5, where it is easily noticeable that the difference is always positive, meaning that the Fresnel coefficient at normal incidence is slightly lower than the effective fraction of reflected light: this is due to the fact that $R_\perp$ and $R_\parallel$ increase with the incidence angle. The low differences for gaussian distribution cases can be explained by the fact that all the rays have a very small incidence angle, thus inducing less changes in $R_\perp$ and $R_\parallel$. On the contrary, uniform mode distribution exhibits larger difference, because of large incidence angles with the same weight as small ones in the calculation. As illustrated by figure 3, distribution based on a Bessel function for equilibrium mode distribution is an intermediate case, a wide distribution but with lower powers at large incidence angles. As one can therefore expect, results for a wide numerical aperture differ more from the normal incidence values: the maximum relative difference is found to be 1.21% for a MMF with 0.5 NA (surrounding medium air, uniform distribution).

It would be useful to determine whether we can use equation (2) rather than equation (14) to deduce the refractive index of the surrounding medium, and the resulting error on the index. For this, inverse calculations are needed: equation (3) and (4) are used with air as the reference medium to retrieve the index of the medium, but values for $P_{r,air}$

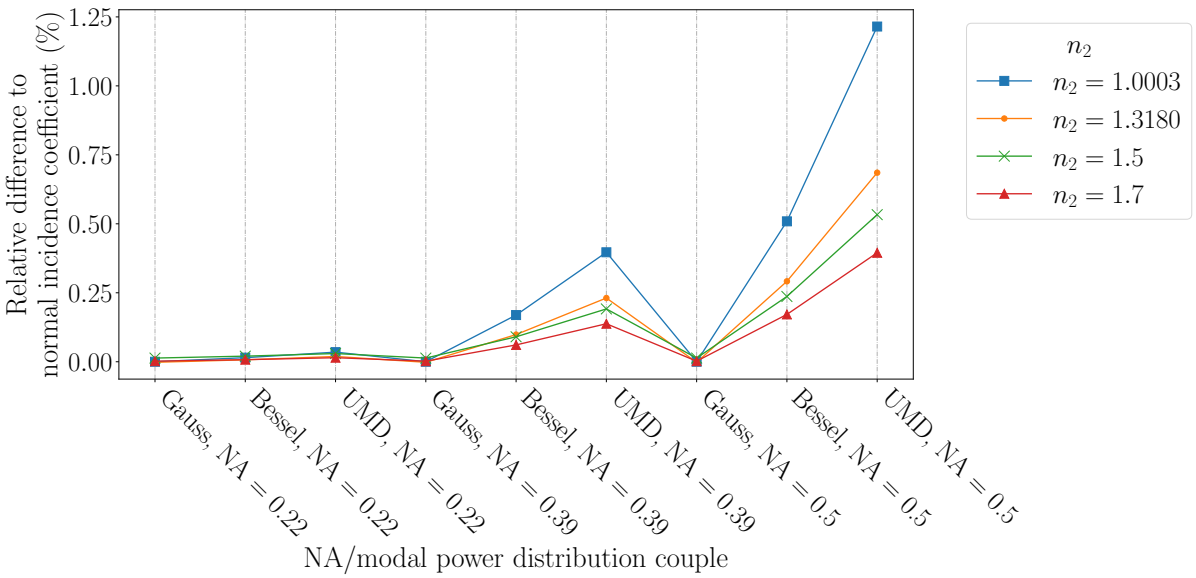

Figure 5: Relative differences (in %) between effective Fresnel power coefficient and normal incidence Fresnel power coefficient, for several fibers, modal power distributions and surrounding medium refractive indexes

and $P_{\mathrm{r,med}}$ are calculated with equation (12). The differences between the indexes deduced with this method and real values are presented in figure 6. Results are very close to the real refractive indexes, even for NA=0.5 and a wide power distribution. The absolute maximum difference on the index is 6×10^{-4} and is once again obtained for the 0.5 NA MMF/uniform distribution configuration, for a theoretical n_2 of 1.7. For the other fibers, the absolute maximum differences on the refractive index are:

- 2×10^{-4} for the 0.39 NA fiber (uniform distribution, theoretical $n_2 = 1.7$)
- 1×10^{-5} for the 0.22 NA fiber (uniform distribution, theoretical $n_2 = 1.7$)

3.2. Study of noise influence on calculated refractive index

From an experimental point of view, measurement noise or detector accuracy can lead to some uncertainties on the deduced refractive index; these uncertainties can be estimated with a statistical analysis. Numerical results obtained with equation (12) will serve as theoretical values for reflected powers P_r, and a white noise w will be applied to simulate experimental results: $P_{r,w} = P_r + w$, where the white noise w is randomly and uniformly chosen in the $[-w_{\max}; w_{\max}]$ range, with $w_{\max}$ being equal to a percentage (either 0.1%, 0.5%, 1%, 2% or 5%) of P_r. For all of the 180 possible configurations (each fiber/power distribution/surrounding medium/noise level quadruple), the process is the following:

1. 15 random noise values are generated for the reflected power in the air, to simulate 15 experimental measurements in the air and calculate an average $P_{r,w}$ in the air.
2. The same procedure in used to obtain an average $P_{r,w}$ in the surrounding medium.
3. The two previous values are used to calculate the ratio of the average noised reflected powers. Using normal incidence hypothesis, a refractive index for the surrounding medium is deduced.
4. The three previous steps are repeated 10 000 times to simulate the complete measurement procedure being done numerous times.

An example of an obtained histogram of the calculated refractive indexes, with its normal probability plot, is presented in figure 7. As illustrated for one case by figure 7b, refractive indexes distribution matches normal distribution: there is

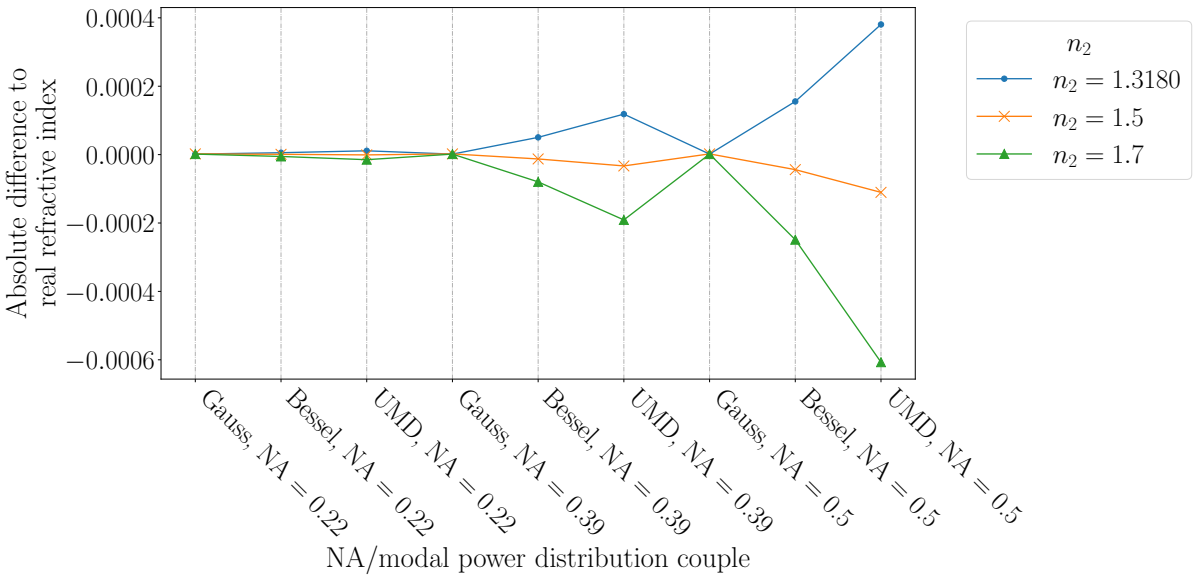

Figure 6: Absolute differences between the numerically deduced refractive indexes and real values

a 99% chance that the calculated refractive index is in the 3σ interval around the average. The 3σ value will therefore be interpreted as the repeatability error on the calculated refractive indexes, and logically increase with noise level, but also with the difference between the fiber refractive index and medium refractive index as illustrated in figure 8.

For fixed values of surrounding medium refractive index or noise level, numerical aperture and modal power distributions appears to have no significant effect on the 3σ interval, as illustrated in figure 9 and 10. These figures also show n_2 influence (at 5% noise level) and noise influence (for $n_2 = 1.7$), respectively.

In the most unfavourable case, i.e. 5% noise and $n_2 = 1.7$, the highest standard deviation found leads to a repeatability error of $\pm 4 \times 10^{-3}$. The other maximum repeatability errors, also obtained for $n_2 = 1.7$, are:

- $\pm 1.6 \times 10^{-3}$ for a 2% noise (value that corresponds to the relative accuracy of the detector that will later be used in the experiments);
- $\pm 8 \times 10^{-4}$ for a 1% noise;
- $\pm 4 \times 10^{-4}$ for a 0.5% noise;
- $\pm 8 \times 10^{-5}$ for a 0.1% noise.

For a 1%, 2% and a 5% noise, the calculated repeatability error is always larger than the error made by using normal incidence formula (approximation error) on a multimode Fresnel sensor. The only cases where the approximation error is larger than the repeatability error are listed in the table 2. Considering that UMD is an unlikely case from an experimental standpoint, this shows that approximation error will most likely be lower than experimental uncertainties, unless the fiber has a large numerical aperture and the noise level is of a few tenth of a percent.

Based on the previous calculations, the normal incidence hypothesis appears to be acceptable, with maximum theoretical differences of the order of 10^{-4}. The statistical analysis also shows that the approximation error made by using normal incidence formula for a Fresnel sensor based on a multimode fiber is in most cases significantly smaller than the repeatability error.

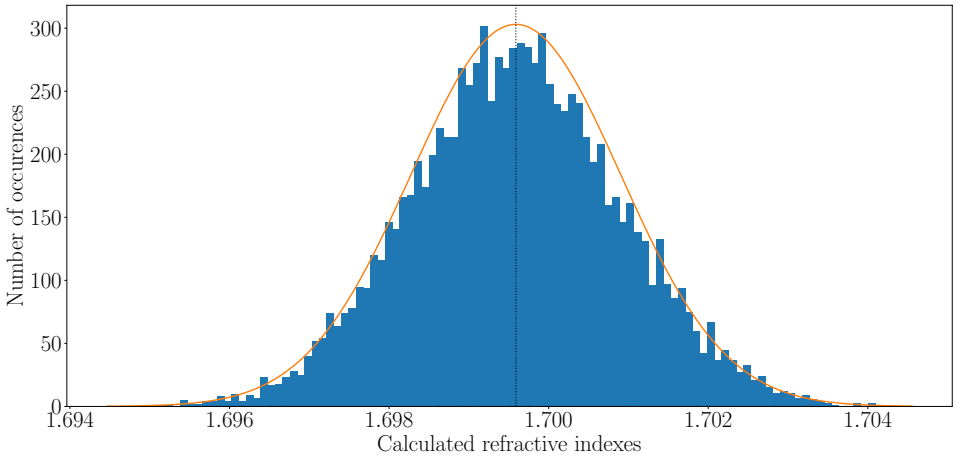

(a) Distribution of the calculated refractive indexes. Normal law parameters: μ = 1.6996 and σ = 0.0013

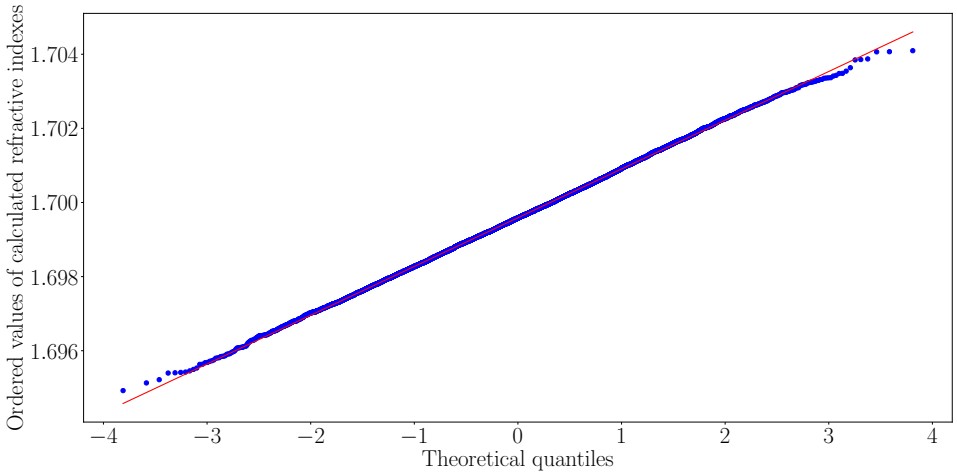

(b) Normal probability plot

Figure 7: Calculated refractive index for the following parameters: Bessel distribution, fiber NA = 0.5, n_2 = 1.7, noise level: 5%

Noise	NA	MPD	n_2	Approximation error	Repeatability error
0.5%	0.5	UMD	1.3180	3.8×10^{-4}	2.2×10^{-4}
0.1%	0.5	Bessel	1.3180	1.5×10^{-4}	4×10^{-5}
0.1%	0.5	UMD	1.3180	3.8×10^{-4}	4×10^{-5}
0.1%	0.39	Bessel	1.3180	5×10^{-4}	4×10^{-5}
0.1%	0.39	UMD	1.3180	1.2×10^{-4}	4×10^{-5}

Table 2: Parameters details for situations where approximation error is larger than repeatability error

4. Experimental confirmation

4.1. Setup and protocol

The experimental setup presented in figure 11 allows for simultaneous comparison between a proven Fresnel sensor based on a SMF and the novel Fresnel sensor based on a MMF, as well as a reference measurement in order to correct the source's potential power variations.

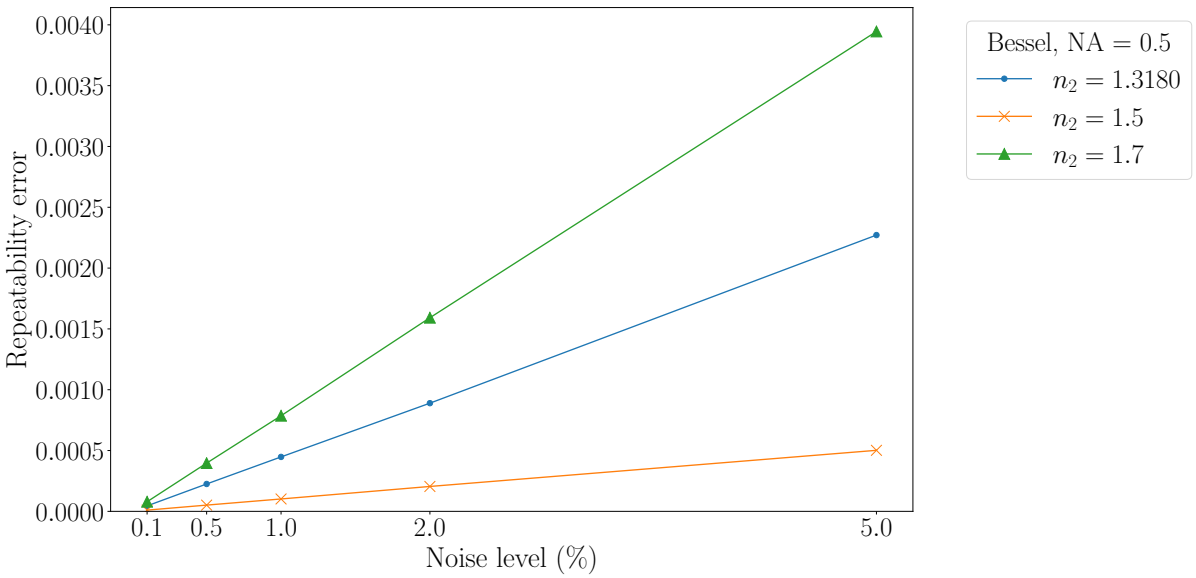

Figure 8: Repeatability error on calculated refractive index, for a 0.5 NA fiber and Bessel modal power distribution

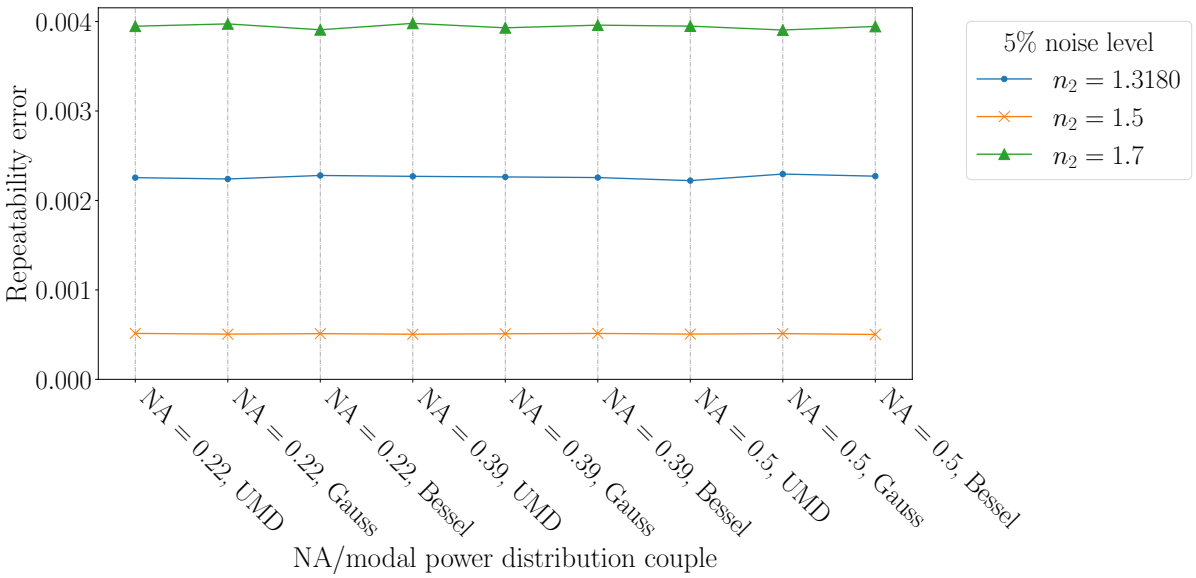

Figure 9: Repeatability error on calculated refractive index, for a fixed 5% noise level and various numerical aperture/power distribution couples

The MMF used is a FG200LEA from Thorlabs, a 0.22 numerical aperture, step-index fiber with a 200 μm diameter core, with both core and cladding made of silica. This fiber was chosen because of its large core diameter, allowing a high number of propagating modes. The number N of modes propagating inside a fiber with a numerical aperture NA and a core radius r, at a wavelength λ, can be approximated by [25]:

$$N = \frac{1}{2}\left(\frac{2\pi r}{\lambda}\mathrm{NA}\right)^2 \tag{16}$$

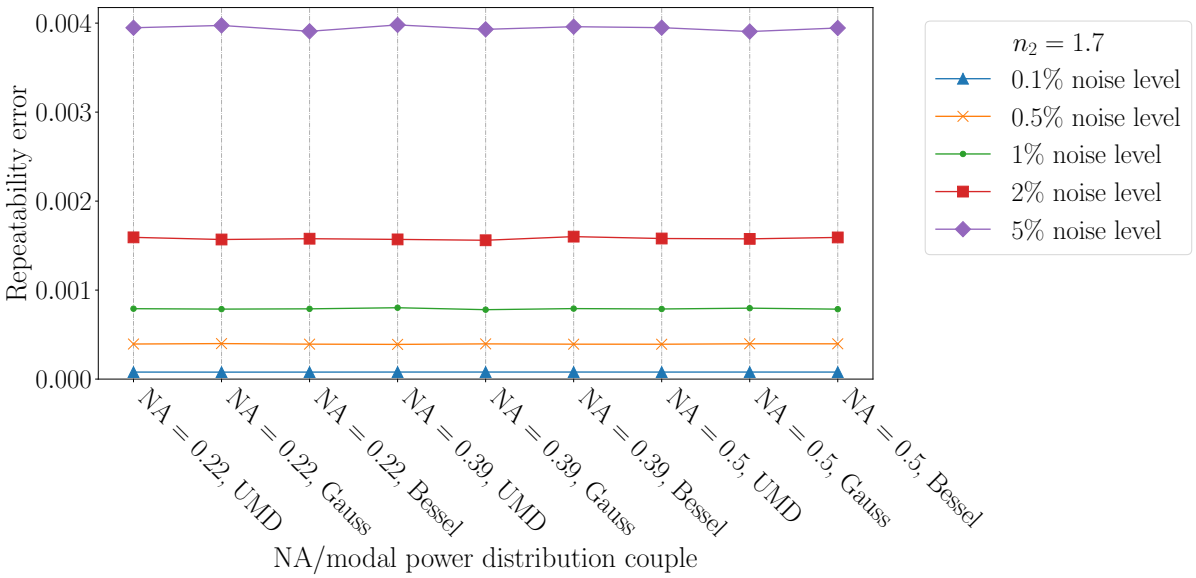

Figure 10: Repeatability error on calculated refractive index, for a fixed $n_2 = 1.7$ and various numerical aperture/power distribution couples

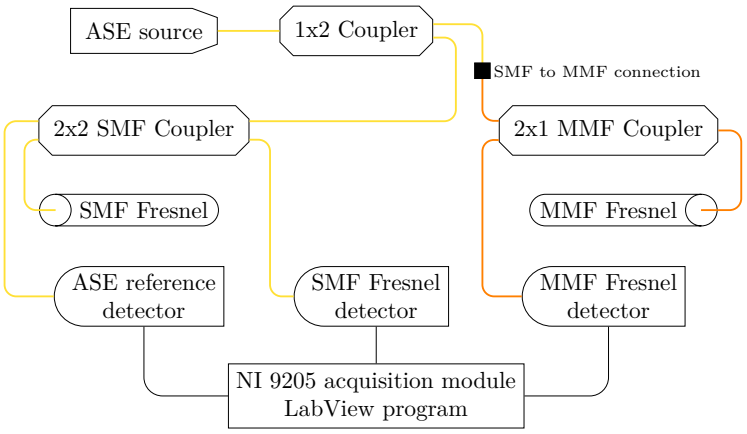

Figure 11: Full Fresnel sensor setup for comparison between SMF and MMF

For the FG200LEA at 1550 nm, $N \approx 4000$. The source is a GN Nettest Fiberwhite ASE source emitting around 1550 nm, and detectors are Newport New Focus with mounted FC-type connectors and 2% relative accuracy. Signal acquisition is realised with a NI-9205, a 16-Bit voltage input module from National Instruments, controlled by a LabView program. Two reference mixtures are studied:

- Distilled water-isopropanol, ranging from 0% to 100% alcohol content with a 10% step;
- Distilled water/sodium chloride, with NaCl concentration ranging from 0g/L to 350g/L with a 50g/L step.

For each of these samples, five measurements of the reflected powers ratio ($P_{\text{r,air}}/P_{\text{r,med}}$) are made to ensure repeatability. A flat-cleaved connector (FC/PC) is used as a sensing head for the MMF, so that the geometry of the sensor stays the same for all measurements, preventing variations due to successive and different cleavings. The power is firstly measured in the air during 20 seconds at a 15 Hz rate, before plunging the fiber in the medium, where the reflected power is also measured during 20 seconds at a 15 Hz rate. Power ratio is calculated using the average power reflected

in the air and in the medium. Between each measurement, fiber tip is cleaned with pure isopropanol and dried with optical cleaning paper. A test measurement of the power reflected in the air is always made before the acquisition of the real data, to ensure that the signal is stable and does not vary because of some isopropanol residues on the connector end. Refractive index is then calculated assuming normal incidence, with equation (3). Measurements are made at a constant temperature, and all results are presented for 25°C. In addition, using the same procedure as described, separate tests were made with the minimal working setup presented in figure 2 but using only multimode fibers components, in order to confirm the repeatability of the measurements, experimental uncertainties and difference to literature and with a multimode fiber only setup.

4.2. Water/isopropanol mixture results

Results for the water/isopropanol mixture based on the full comparison setup between SMF and MMF are presented in figure 12, where the non-linear evolution of the refractive index is clearly visible, as it is one of the numerous properties of the mixture that does not evolve linearly with the alcohol content [33]. Good agreement is found with literature values from [34] for refractive index evolution with alcohol content, shifted at 1550 nm with values from [30] for water and pure isopropanol refractive index at 1550 nm: a maximum refractive index difference of 1.2×10^{-3}, which corresponds to a relative difference of 0.09%, is found. The uncertainties on the measured refractive indexes are based on both Type A and Type B evaluations as recommended in [35], and maximum values are found to be $u_{c,\mathrm{SMF}} = 7 \times 10^{-5}$ for the Fresnel based on SMF, and $u_{c,\mathrm{MMF}} = 8 \times 10^{-5}$ for the Fresnel based on MMF. These values are larger than the approximation error made by using the normal incidence formula: for a 0.22 NA fiber and water, the approximation error from the numerical calculation was found to be of the 10^{-5} to 10^{-6} order. In this work, refractive index from the Fresnel on SMF can be considered as a reference value. It is noteworthy than the maximum difference between measured refractive index with SMF and MMF is 5×10^{-4}, as illustrated at the bottom of figure 12, which is the same order as the 3σ interval from the statistical analysis: for a 2% noise level and $n_{2,\mathrm{th}} = 1.3180$, a repeatability error of 9×10^{-4} was found. Results for the multimode fiber only setup present no difference from the previous results: the maximum refractive index difference to literature is 1.2×10^{-3} (relative difference of 0.09%), and the maximum uncertainty on the measured refractive indexes is also $u_{c,\mathrm{MMF\ only}} = 8 \times 10^{-5}$.

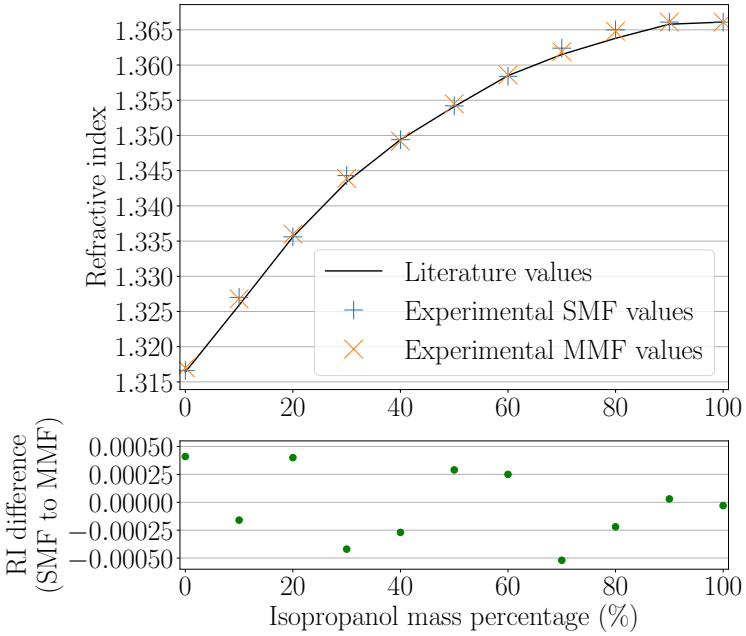

Figure 12: Literature [30] and measured (SMF/MMF comparison setup) refractive indexes of water/isopropanol solution (top), and refractive index (RI) differences between Fresnel on SMF and MMF (bottom)

4.3. Water/sodium chloride results

Results for water/sodium chloride mixture based on the full comparison setup between SMF and MMF are presented in figure 13. Once again, good agreement is found with literature values from [30], with a maximum refractive index difference of 8×10^{-4}, which corresponds to a relative difference of 0.06%. Maximum uncertainties on the measured refractive indexes, based on both Type A and Type B evaluations as recommended in [35], are found to be $u_{c,\mathrm{SMF}} = 1.1 \times 10^{-4}$ for the Fresnel based on SMF, and $u_{c,\mathrm{MMF}} = 8 \times 10^{-5}$ for the Fresnel based on MMF, values which are larger than the approximation error made by using the normal incidence formula. The maximum difference between measured refractive index with SMF and MMF is 8×10^{-4}, as illustrated at the bottom of figure 13, once again the same order as the 3σ interval from the statistical analysis. Once again, results for the multimode fiber only setup present no significant difference from the comparison setup results: the maximum refractive index difference to literature is 1.3×10^{-3} (relative difference of 0.1%), and the maximum uncertainty on the measured refractive indexes is also $u_{c,\mathrm{MMF\ only}} = 8 \times 10^{-5}$.

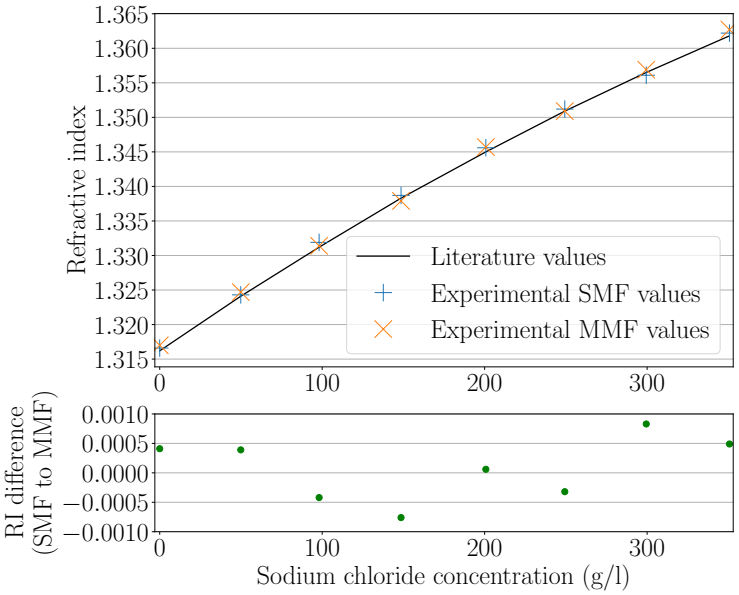

Figure 13: Literature [30] and measured (SMF/MMF comparison setup) refractive indexes of water/sodium chloride solution (top), and refractive index (RI) differences between Fresnel on SMF and MMF (bottom)

4.4. Performance and applications comparison

Performances of the proposed sensor, in terms of measurement uncertainty and refractive index range, are well within the range of other measurement systems existing in the literature, as displayed in table 3, which further confirms its relevance for refractive index measurement. One advantage on the proposed system in this work is its simplicity, as it requires almost no preliminary operations, except for fiber cleaving and obvious system assembly. Using an OTDR as a combined source and interrogator [36] can further simplifies the system, as coupler and external acquisition systems are not longer needed. Comparing a high-end OTDR to a simple laser source and photodiode detector, such a system will however most likely be more expensive. Commercially available refractometers such as those in table 3 offer the advantage of being ready to use, but contrary to the Fresnel sensor, can not be used for *in-situ* measurements in liquids and require a sample extraction. Most of them, especially handheld refractometers, work in the visible range, and refractometer measurements in the inrafred often requires a tailored setup such as the one in [30]. Interferometric methods [37, 38] are used to measure transparent samples, and are well-known for their high sensibility. However, they almost always require an extensive preliminary work in order to properly calibrate the interferometer. Fresnel sensor, on the other end, can be used quickly as it only needs a reference measurement in the air ; it can also measure the refractive index of absorbing medium with an high imaginary part in its complex refractive index, assuming the

imaginary part is known [39]. For a transparent sample, interferometry and some refractometers can be used on a solid sample, whereas Fresnel sample can only be used on solid sample if it was possible to insert the fiber in the sample beforehand, e. g. before epoxy curing or medium freezing.

Setup	RI range studied	Wavelength (nm)	Uncertainty ($\times 10^{-4}$)	Source
Fresnel on SMF, InGaAs Detector	1.31 - 1.36	1550	1.1	This work
Fresnel on MMF, InGaAs Detector	1.31 - 1.36	1550	0.8	This work
Fresnel SMF with OTDR	1.35 - 1.45	1550	2.58	[36]
Fresnel SMF with multi-wavelength OTDR	1.33 - 1.46	1550, 1625	1.7	[17]
Fresnel SMF with photodiode	1.3 - 1.6	1550	3.82 - 7.33	[40]
Prism coupling refractometer	1.3 - 1.6	1550	2	[40]
Infrared refractometer with CCD camera	1.31 - 1.49	1550	1	[30]
Vis-NIR white light interferometry	1.41 - 1.5	400 - 1000	2	[37]
Fiber Bragg Grating and Fabry-Perot Interferometer	1.00 - 1.60	1550	4.50 - 7.17	[41]
Modified Michelson interferometer	1.33 - 1.47	632,8	2	[38]
Metler Toledo Excellence R5	1.32 - 1.58	Unknown	0.2	Manufacturer data
Metler Toledo 30GS	1.32 - 1.65	Unknown	5	Manufacturer data
Bellingham + Stanley RFM712-M	1.33 - 1.42	Unknown	1	Manufacturer data

Table 3: Performance comparison of refractive index (RI) measurement systems in the literature and commercial systems

5. Conclusion

This paper showed that is it possible to use a MMF as Fresnel sensor, and that normal incidence hypothesis can be made to deduce the refractive index of the surrounding medium without significant precision loss. Numerical study showed that even with this approximation, a refractive index measurement with a precision up to 10^{-4} can still be achieved in most cases, as the effects only become noticeable for large numerical apertures and wide power distributions. The experimental study confirmed these claims, using a Fresnel sensor based on a FG200LEA multimode fiber and on a single-mode fiber for comparison, to measure alcohol and sodium chloride content in a water solution. Good agreement was found between the results and reference values from the literature, with a relative difference between the experimental and literature refractive indexes of only 0.09% for the isopropanol mixture and 0.1% for the sodium chloride solution. No significant difference was found between the two experimental setups used (SMF/MMF comparison setup and MMF only setup), whether it is for experimental uncertainties, absolute measured refractive indexes values or differences to literature. The overall maximum uncertainty on the refractive index of this work is 1.1×10^{-4}, which is larger than the error made by using the normal incidence hypothesis for a Fresnel based on a multimode fiber.

Acknowledgement

This project was co-funded by the European Regional Development Fund and Région Pays de la Loire under the CIPITAP project.

References

[1] M. Born, E. Wolf, A. B. Bhatia, P. C. Clemmow, D. Gabor, A. R. Stokes, A. M. Taylor, P. A. Wayman, W. L. Wilcock, Principles of Optics: Electromagnetic Theory of Propagation, Interference and Diffraction of Light, 7th Edition, Cambridge University Press, 1999. doi:10.1017/CBO9781139644181.

[2] T. Okoshi, Optical Fibers, Academic Press, 1982.

[3] E. Hecht, Optics, 5th Edition, Pearson, 2017.

[4] A. Sihvola, Electromagnetic Mixing Formulas and Applications, The Institution of Engineering and Technology, 2008.

[5] G. Burton, L. Melo, S. Warwick, M. Jun, B. Bao, D. Sinton, P. Wild, Fiber refractometer to detect and distinguish carbon dioxide and methane leakage in the deep ocean, International Journal of Greenhouse Gas Control 31 (2014) 41–47. doi:10.1016/j.ijggc.2014.09.015.
URL http://dx.doi.org/10.1016/j.ijggc.2014.09.015

[6] X. Ning, C. Zhao, F. Shi, S. Jin, Multipoint chemical vapor measurement by zeolite thin film-coated Fresnel reflection-based fiber sensors with an Array-Waveguide Grating, Sensors and Actuators, B: Chemical 227 (2016) 533–538. doi:10.1016/j.snb.2015.12.059.
URL http://dx.doi.org/10.1016/j.snb.2015.12.059

[7] P. Q. Zhu, J. J. Wang, F. Rao, C. Yu, G. Zhou, X. G. Huang, Differential Fresnel-reflection-based fiber biochemical sensor with temperature self-compensation for high-resolution measurement of Cd 2+ concentration in solution, Sensors and Actuators, B: Chemical 282 (November 2018) (2019) 644–649. doi:10.1016/j.snb.2018.11.126.
URL https://doi.org/10.1016/j.snb.2018.11.126

[8] A. Cusano, G. Breglio, M. Giordano, A. Calabrò, A. Cutolo, L. Nicolais, Optoelectronic sensor for cure monitoring in thermoset-based composites, Sensors and Actuators, A: Physical 84 (3) (2000) 270–275. doi:10.1016/S0924-4247(00)00361-7.

[9] S. Vacher, J. Molimard, H. Gagnaire, A. Vautrin, A Fresnel's reflection optical fiber sensor for thermoset polymer cure monitoring, Polymers and Polymer Composites 12 (4) (2004) 269–276.

[10] X.-A. Aduriz, C. Lupi, N. Boyard, J. L. Bailleul, D. Leduc, V. Sobotka, N. Lefèvre, X. Chapeleau, C. Boisrobert, D. Delaunay, Quantitative control of RTM6 epoxy resin polymerisation by optical index determination, Composites Science and Technology 67 (15-16) (2007) 3196–3201. doi:10.1016/j.compscitech.2007.04.008.

[11] R. Grangeat, M. Girard, C. Lupi, D. Leduc, F. Jacquemin, Measurement of the local water content of an epoxy adhesive by fiber optic sensor based on Fresnel reflection, Mechanical Systems and Signal Processing 91. doi:10.1016/j.ymssp.2019.106439.
URL https://doi.org/10.1016/j.ymssp.2019.106439

[12] W. Han, M. Rebow, D. Liu, G. Farrell, Y. Semenova, Q. Wu, Optical fiber Fresnel reflection sensor for direct detection of the solid-liquid phase change in n-octadecane, Measurement Science and Technology 29 (12). doi:10.1088/1361-6501/aaeabb.

[13] J. Y. Li, X. G. Huang, W. Xu, D. R. Xiao, Z. B. Zhong, A fiber-optic pH sensor based on relative Fresnel reflection technique and biocompatible coating, Optical Fiber Technology 20 (1) (2014) 28–31. doi:10.1016/j.yofte.2013.11.002.
URL http://dx.doi.org/10.1016/j.yofte.2013.11.002

[14] J. H. Chen, X. G. Huang, W. X. He, J. Tao, A parallel-multipoint fiber-optic temperature sensor based on Fresnel reflection, Optics & Laser Technology 43 (8) (2011) 1424–1427. doi:10.1016/j.optlastec.2011.04.012.
URL http://dx.doi.org/10.1016/j.optlastec.2011.04.012

[15] J. R. Zhao, X. G. Huang, J. H. Chen, A Fresnel-reflection-based fiber sensor for simultaneous measurement of liquid concentration and temperature, Journal of Applied Physics 106 (8) (2009) 1–6. doi:10.1063/1.3239851.

[16] E. Fujiwara, R. T. Takeishi, A. Hase, E. Ono, J. S. Santos, C. K. Suzuki, Real-time optical fibre sensor for hydro-alcoholic solutions, Measurement Science and Technology 21 (9). doi:10.1088/0957-0233/21/9/094035.

[17] K. Yüksel, Optical fiber sensor system for remote and multi-point refractive index measurement, Sensors and Actuators, A: Physical 250 (2016) 29–34. doi:10.1016/j.sna.2016.09.003.
URL http://dx.doi.org/10.1016/j.sna.2016.09.003

[18] R. Grangeat, M. Girard, C. Lupi, D. Leduc, F. Jacquemin, Revealing of interphases in bonded joints with a fiber optic sensor based on Fresnel reflection, International Journal of Adhesion and Adhesives 91 (February) (2019) 12–18. doi:10.1016/j.ijadhadh.2019.02.009.
URL https://doi.org/10.1016/j.ijadhadh.2019.02.009

[19] T. Gordelier, P. R. Thies, G. Rinaldi, L. Johanning, Investigating polymer fibre optics for condition monitoring of synthetic mooring lines, Journal of Marine Science and Engineering 8 (2). doi:10.3390/jmse8020103.
URL https://www.mdpi.com/2077-1312/8/2/103

[20] J. Villatoro, D. Monzon-Hernandez, D. Talavera, High resolution refractive index sensing with cladded multimode tapered optical fibre, Electronics letters 40 (2) (2004) 106–107. doi:10.1049/el:20040069.

[21] H. Apriyanto, G. Ravet, O. D. Bernal, M. Cattoen, H. C. Seat, V. Chavagnac, F. Surre, J. H. Sharp, Comprehensive Modeling of Multimode Fiber Sensors for Refractive Index Measurement and Experimental Validation, Scientific Reports 8 (1) (2018) 5912. doi:10.1038/s41598-018-24153-0.

[22] L. Bilro, N. Alberto, J. L. Pinto, R. N. Nogueira, A simple and low-cost cure monitoring system based on a side-polished plastic optical fibre, Measurement Science and Technology 21 (11). doi:10.1088/0957-0233/21/11/117001.

[23] C.-B. Kim, C. B. Su, Measurement of the refractive index of liquids at 1.3 and 1.5 micron using a fibre optic Fresnel ratio meter, Measurement Science and Technology 15 (9) (2004) 1683–1686. doi:10.1088/0957-0233/15/9/002.

[24] D. Gloge, Optical Power Flow in Multimode Fibers, Bell System Technical Journal 51 (8) (1972) 1767–1783. doi:10.1002/j.1538-7305.1972.tb02682.x.

[25] O. Ziemann, J. Krauser, P. E. Zamzow, W. Daum, POF Handbook, Springer-Verlag, 2008. doi:10.1007/978-3-540-76629-2.

[26] S. Savović, A. Djordjevich, Calculation of the coupling coefficient in strained step index plastic optical fibers, Applied Optics 47 (27) (2008) 4935–4939. doi:10.1364/AO.47.004935.

[27] M. Rousseau, L. Jeunhomme, Numerical Solution of the Coupled-Power Equation in Step-Index Optical Fibers, IEEE Transactions on Microwave Theory and Techniques 25 (7) (1977) 577–585. doi:10.1109/TMTT.1977.1129162.

[28] J. W. Fleming, Dispersion in GeO_2-SiO_2 glasses, Applied Optics 23 (24) (1984) 4486–4493. doi:10.1364/AO.23.004486.
URL https://doi.org/10.1364/AO.23.004486
[29] G. M. Hale, M. R. Querry, Optical Constants of Water in the 200-nm to 200-μm Wavelength Region, Applied Optics 12 (3) (1973) 555. doi:10.1364/ao.12.000555.
[30] J. E. Saunders, C. Sanders, H. Chen, H.-P. Loock, Refractive indices of common solvents and solutions at 1550 nm, Applied Optics 55 (4) (2016) 947–953. doi:10.1364/ao.55.000947.
[31] S. A. Khodier, Refractive index of standard oils as a function of wavelength and temperature, Optics & Laser Technology 34 (2) (2002) 125 – 128. doi:https://doi.org/10.1016/S0030-3992(01)00101-3.
URL http://www.sciencedirect.com/science/article/pii/S0030399201001013
[32] E. S. Larsen, R. Meyrowitz, A. J. C. Wilson, Measurement of refractive index, American Cancer Society, 2006, Ch. 3.3, pp. 160–161. arXiv:https://onlinelibrary.wiley.com/doi/pdf/10.1107/9780955360206000587, doi:10.1107/9780955360206000587.
URL https://onlinelibrary.wiley.com/doi/abs/10.1107/9780955360206000587
[33] V. I. Kuchuk, I. Y. Shirokova, E. V. Golikova, Physicochemical properties of water-alcohol mixtures of a homological series of lower aliphatic alcohols, Glass Physics and Chemistry 38 (5) (2012) 460–465. doi:10.1134/S1087659612050057.
[34] K. Y. Chu, A. R. Thompson, Densities and Refractive Indices of Alcohol-Water Solutions of n-Propyl, Isopropyl, and Methyl Alcohols, Journal of Chemical and Engineering Data 7 (3) (1962) 358–360. doi:10.1021/je60014a011.
[35] Evaluation of measurement data - Guide to the expression of uncertainty in measurement, Joint Committee for Guides in Metrology, 2008.
[36] J. Yuan, C. Zhao, M. Ye, J. Kang, Z. Zhang, S. Jin, A Fresnel reflection-based optical fiber sensor system for remote refractive index measurement using an OTDR, Photonic Sensors 4 (1) (2014) 48–52. doi:10.1007/s13320-013-0131-6.
[37] Y. Arosa, C. D. Rodríguez Fernández, E. López Lago, A. Amigo, L. M. Varela, O. Cabeza, R. de la Fuente, Refractive index measurement of imidazolium based ionic liquids in the Vis-NIR, Optical Materials 73 (2017) 647–657. doi:10.1016/j.optmat.2017.09.028.
[38] S. R. Kachiraju, D. A. Gregory, Determining the refractive index of liquids using a modified Michelson interferometer, Optics and Laser Technology 44 (8) (2012) 2361–2365. doi:10.1016/j.optlastec.2012.04.020.
URL http://dx.doi.org/10.1016/j.optlastec.2012.04.020
[39] S. Pu, X. Chen, Y. Chen, W. Liao, L. Chen, Y. Xia, Measurement of the refractive index of a magnetic fluid by the retroreflection on the fiber-optic end face, Applied Physics Letters 86 (17) (2005) 1–3. doi:10.1063/1.1905808.
[40] J. Oelhafen, T. Mayr, F. Dorner, K. Moutzouris, J. Roths, K. Drechsler, Fiber Optic Measurement System for Fresnel Reflection Sensing: Calibration, Uncertainty, and Exemplary Application in Temperature-Modulated Isothermal Polymer Curing, Journal of Lightwave Technology 36 (4) (2018) 939–945. doi:10.1109/JLT.2017.2757525.
[41] O. Rodríguez-Quiroz, C. E. Domínguez-Flores, D. Monzón-Hernández, E. Morales-Narváez, V. P. Minkovich, D. López-Cortés, Unambiguous refractive-index measurement in a wide dynamic-range using a hybrid fiber Fabry-Perot interferometer assisted by a fiber Bragg grating, Optics and Laser Technology 128 (2020) 106236. doi:10.1016/j.optlastec.2020.106236.
URL https://doi.org/10.1016/j.optlastec.2020.106236